



**RESEARCH ARTICLE**

# 3D bioprinting of gellan gum-based hydrogels tethered with laminin-derived peptides for improved cellular behavior

Omar Alheib<sup>1,2</sup>  | Lucilia P. da Silva<sup>1,2</sup> | Yun Hee Youn<sup>1,2,3</sup>  | Il Keun Kwon<sup>3</sup> | Rui L. Reis<sup>1,2,3</sup> | Vitor M. Correlo<sup>1,2</sup>

<sup>1</sup>3B's Research Group, I3Bs – Research Institute on Biomaterials, Biodegradables and Biomimetics, University of Minho, Headquarters of the European Institute of Excellence on Tissue Engineering and Regenerative Medicine, Guimarães, Portugal

<sup>2</sup>CVS/3B's-PT Government Associate Laboratory, Guimarães, Portugal

<sup>3</sup>Department of Dental Materials, School of Dentistry, Kyung Hee University, Seoul, Republic of Korea

**Correspondence**

Lucilia P. da Silva and Vitor M. Correlo, 3B's Research Group, I3Bs – Research Institute on Biomaterials, Biodegradables and Biomimetics, University of Minho, Headquarters of the European Institute of Excellence on Tissue Engineering and Regenerative Medicine, AvePark, Parque de Ciência e Tecnologia, Zona Industrial da Gandra, 4805-017 Barco, Guimarães, Portugal.

Email: [lucilia.silva@i3bs.uminho.pt](mailto:lucilia.silva@i3bs.uminho.pt) (L. P. S.)

Email: [vitorcorrelo@i3bs.uminho.pt](mailto:vitorcorrelo@i3bs.uminho.pt) (V. M. C.)

**Funding information**

CEEC Individual, Grant/Award Number: 2020.01541.CEECIND/CP1600/CT0024; Fundação para a Ciência e a Tecnologia, Grant/Award Number: PD/BD/128090/2016

**Abstract**

The treatment of skeletal muscle defects is still a topic of noteworthy concern since surgical intervention is not capable of recovering muscle function. Herein, we propose myoblasts laden in laminin-inspired biofunctionalized gellan gum hydrogels as promising tissue-engineered skeletal muscle surrogates. Gellan gum-based hydrogels were developed by combining native gellan gum (GG) and GG tethered with laminin-derived peptides (CIKVAVS (V), KNRLTIELEVRTC (T) or RKRLQVQLSIRTC (Q)), using different polymer content (0.75%–1.875%). Hydrogels were characterized in terms of compressive modulus, molecules trafficking, and C2C12 adhesion. Hydrogels with higher polymeric content (1.125%–1.875%) showed higher stiffness whereas hydrogels with lower polymer content (0.75%–1.125%) showed higher fluorescein isothiocyanate-dextran molecules diffusion. Cell spreading was achieved regardless of the laminin-derived peptide but preferred in hydrogels with higher polymer content (1.125%–1.875%). Taken together, hydrogels with 1.125% of polymer content were selected for printability analysis. GG-based inks showed a non-newtonian, shear-thinning, and thixotropic behavior suitable for printing. Accordingly, all inks were printable, but inks tethered with T and Q peptides presented some signs of clogging. Cell viability was affected after printing but increased after 7 days of culture. After 7 days, cells were spreading but not showing significant signs of cell–cell communications. Therefore, cell density was increased, thus, myocytes loaded in V-tethered GG-based inks showed higher cell–cell communication, spreading morphology, and alignment 7, 14 days post-printing. Overall, myoblasts laden in laminin-inspired biofunctionalized GG-based hydrogels are a promising skeletal muscle surrogate with the potential to be used as *in vitro* model or explored for further *in vivo* applications.

**KEYWORDS**

cell encapsulation, gellan gum, laminin, tissue engineering

**1 | INTRODUCTION**

Skeletal muscles are highly organized tissues and play an important role in generating forces and supporting body posture.<sup>1</sup> When used improperly, muscles will be prone to injuries among high demand

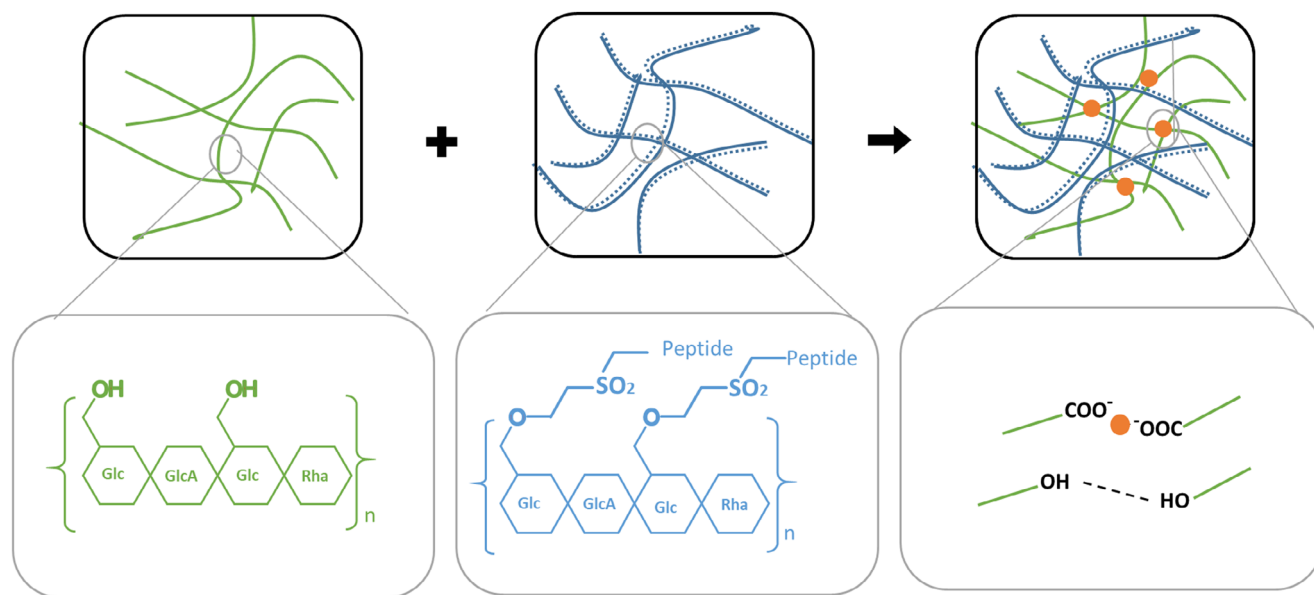
activities such as sport athletes, or even in the daily basis of physical activity.<sup>2</sup> Despite their intrinsic regeneration capability,<sup>3</sup> self-renewing is restricted to small injuries and based on a limited amount of a satellite cell pool. Thus, upon skeletal muscle injury, the muscular function is deteriorated due to the altered response to injury signals,<sup>4,5</sup> which

results in a prolonged healing time especially among aged people.<sup>6</sup> At the moment, surgery is the only available solution to treat muscular injuries and patients limitedly regain muscular activity.<sup>7</sup> Thus, there is a critical need of functional skeletal muscle surrogates to replace the damaged tissues, as well as new therapies and skeletal muscle models to test the efficacy of these therapeutics for skeletal muscle regeneration.

Hydrogels present an optimum environment to promote cellular function and response.<sup>8</sup> On one side, hydrogels present a high water content that closely resembles the water amount in the extracellular tissue.<sup>9</sup> On the other side, hydrogels can be developed in a wide range of stiffness mimicking the mechanics of the native tissue.<sup>10</sup> Beyond these interesting properties, hydrogels can be further bioengineered to better mimic the native tissue environment and trigger particular cell responses. Thus, it is not surprising that researchers have selected these matrices to culture myocytes. Some works have already shown the proliferation, differentiation, and alignment of myoblasts on the top of hydrogels.<sup>11,12</sup> Nonetheless, as 2D cell culture does not necessarily mimic the native 3D microenvironment complexity,<sup>13</sup> authors started to explore myocytes behavior within the 3D hydrogels. Accordingly, 3D bioprinting has emerged as a great potential approach for automated engineering of 3D tissues surrogates with high complexity, reproducibility, and shape fidelity.<sup>14</sup> In the context of skeletal muscle engineering, it is capable of controlling the spatial dimensions

of printed myofibers in order to mimic their hierarchical organization within bundles. This technology has inspired some authors to engineer skeletal muscle surrogates. As such, Distler et al used a blend of oxidized alginate and gelatin hydrogel as an ink to bioprint C2C12.<sup>15</sup> The bioprinted construct inspired cellular differentiation and alignment. In addition, a blend of gelatin, alginate and collagen was used to bioprint C2C12.<sup>16</sup> Post-printing, more than 80% of the cells were alive, however, cells were poorly spreading, and their morphology was not evolving into myotubes. Overall, despite some interesting results in what regards to cell alignment and differentiation using C2C12 laden in oxidized alginate/gelatin hydrogels,<sup>15</sup> the bioprinted constructs still present limited functionality.

Herein, we hypothesized that printing hydrogels tethered with specific peptides that emulate the muscular ECM would provide a more accurate microenvironment for skeletal muscle cells' maturity. We selected gellan gum (GG) to develop gellan gum-based hydrogels, since it is a natural, biocompatible and biodegradable biomaterial which was used to regenerate multiple tissues, such as skin,<sup>17-20</sup> bone,<sup>21</sup> and more recently started to be explored for skeletal muscle engineering.<sup>12,22,23</sup> Moreover, GG presents adequate properties for cell encapsulation (i.e., cell dispersion in low viscous solutions and crosslinking at a physiological environment) and for printing owed to its rheological features (non-newtonian, shear-thinning and thixotropic behavior) and dual crosslinking (temperature and cations). Three different laminin-derived



Legend:

— Gellan Gum (GG) — Divinyl sulfone modified gellan gum (GGDVS) ..... Laminin-derived peptide  
 - - - - - Hydrogen bridge • Cations

**FIGURE 1** Schematic representation of gellan gum-based hydrogels tethered with laminin-derived peptides, their main components and crosslinking mechanism. Gellan gum-based hydrogels are prepared through the combination of gellan gum (GG) and divinyl sulfone modified gellan gum (GGDVS) biofunctionalized with laminin-derived peptides (Q, V and T). A semi-interpenetrating polymer network results from this combination since GGDVS-peptide remains uncrosslinked, but entangled within a crosslinked GG polymeric network. The crosslinking of GG polymeric chains occurs by GG sol-gel transition during the decrease of temperature and formation of hydrogen bridges, as well as, by the addition of cations as they attract the negative charged carboxylate groups of GG.

peptides, RKRLQVLSIRT (Q), KNRLTIELEVRT (T), and IKVAV (V), were selected to tether to GG through divinyl sulfone (DVS) chemically attached moieties (Figure 1).<sup>24</sup> Different surface receptors mediate the interactions between myoblasts and the above-mentioned peptides: “Syndican-1,” a heparan sulfate proteoglycan receptor, mediates the interaction between Q or T peptides and cell surface<sup>25,26</sup>; the integrin receptors “ $\alpha3\beta1/\alpha6\beta1$ ” mediate the interaction between V peptide and the cell surface.<sup>27,28</sup> Q peptide has previously shown to enhance C2C12 attachment and differentiation,<sup>12</sup> whereas T peptide has been reported to improve C2C12 adhesion.<sup>12</sup> IKVAV, well known for promoting cell attachment,<sup>29</sup> was included in our study as a reference peptide from the laminin.

After previously showing that the adhesion, proliferation and differentiation of myocytes was enhanced on top of the Q-biofunctionalized hydrogels,<sup>12</sup> herein we aimed go further and study myocytes behavior inside the biofunctionalized hydrogels, a more relevant environment. To this aim, skeletal muscle cells (C2C12) were encapsulated within the different hydrogels and their adhesion evaluated after 7 days. In order to infer about the different cell behavior within the different hydrogel formulations, hydrogels were characterized in terms of mechanical properties and molecules diffusion. Afterwards, we investigated the printability of the developed hydrogels and further evaluated the behavior of the encapsulated cells up to 14 days post-printing.

## 2 | MATERIALS AND METHODS

### 2.1 | Biofunctionalization of gellan gum with laminin-derived peptides

Gellan gum (GG) was functionalized following an established protocol.<sup>24</sup> Briefly, surplus amount of divinyl sulfone (DVS, Sigma-Aldrich) was added dropwise to 0.25% (wt/vol) GG (Gelzan™ CM Gelrite®, Sigma-Aldrich) solution (molar ratio 30:1) under vigorous stirring. The mixture was protected from light and allowed to react at room temperature (RT). After an hour of reaction, the reaction was stopped, and the GGDVS solution was dialyzed against deionized water in a 14-kDa cutoff dialysis tube with 33 mm (1.3 IN) flat width (Sigma-Aldrich) for 4 days to remove unreacted DVS. Diethyl ether was used to eliminate any additional byproducts. As a final step of reaction, GGDVS was freeze-dried and stored at  $-20^{\circ}\text{C}$  until the time of use.

GGDVS (5, 7.5, 10 or 12.5 mg/ml) was dissolved in 0.5 M of Sucrose (Sigma, USA) at pH 9. Then, GGDVS was reacted with the peptide of interest (RKRLQVLSIRT (Q), KNRLTIELEVRT (T) or CIKVAVS (V), 800  $\mu\text{M}$ ,  $\geq 95\%$  purity, GeneCust France) for 1 h, at RT, under agitation.

### 2.2 | Efficiency of conjugation of Q, V and T peptides to GGDVS

Protein assay kit (23,235#, Thermo Scientific™) was used to evaluate the efficiency of conjugation of Q, V and T peptides to GGDVS.

Accordingly, after reaction of GGDVS (10 mg/ml) with the peptide (800  $\mu\text{M}$ ), the GGDVS-peptide was dialyzed for 24 h and freeze-dried. GGDVS-peptide samples were prepared at 0.5, 0.2 and 0.1 mg/ml and mixed with the bicinchoninic acid (BCA) reagent. A stock solution (2 mg/ml) of each peptide was used to prepare a series of standard solution ranging from 0.5 to 200  $\mu\text{g}/\text{ml}$  in triplicates. After 2 h of incubation with bicinchoninic acid (BCA) at  $37^{\circ}\text{C}$ , a spectrophotometer was utilized to measure samples absorbance at a wavelength of 562 nm.

### 2.3 | Gellan gum-based hydrogel preparation

GG was dissolved in 50% of the total volume in water, at  $90^{\circ}\text{C}$ . After 30 min, the temperature was lowered to  $37^{\circ}\text{C}$ . GG was dissolved in 40% of the final volume in 0.5 M sucrose solution pH 9, at  $37^{\circ}\text{C}$ , for 20 min with stirring. The peptide was dissolved in 10% of the final volume in 0.5 M sucrose solution pH 9, at RT, instantaneously when contacting with the solution. In parallel, GGDVS and peptides were dissolved at RT in 50% of the final volume of 0.5 M sucrose solution, pH 9. After dissolution of all the components, the peptide solution was added to the GGDVS solution and left with stirring for 1 h, at RT, for the reaction to occur. After this period, equal volumes of GGDVS-peptide and GG were mixed at  $37^{\circ}\text{C}$  by pipetting (up and down) using a pipette for viscous solutions. A desired amount of this pre-hydrogel solution (please see volume amount below for each assay) was casted into a well-plate and the crosslinking occurred by lowering the temperature below  $37^{\circ}\text{C}$  and through the addition of cation-containing high glucose Dulbecco's Modified Eagle Medium (DMEM, Sigma, USA). Four different gellan gum-based hydrogel formulations were prepared by tailoring the concentration of GG and GGDVS, as indicated in the following Table 1.

### 2.4 | Compressive testing

Gellan gum-based hydrogels prepared through casting (500  $\mu\text{l}$ , 10 mm in diameter, 5 mm in height) or printing (10 x 10 x 0.4 mm) were incubated at  $37^{\circ}\text{C}$  in HG-DMEM for 48 h prior testing. An Instron 5543 universal mechanical testing equipment (Instron Int. Ltd., USA) was used to evaluate the compressive stiffness of the samples. The analysis was performed at RT up to 60% final strain with a 0.01 N preload force, and 1 mm per 1 min strain rate. The linear area (0%–3% of strain) of the curve between stress and strain was considered to

**TABLE 1** Gellan gum-based hydrogel formulations

	Hydrogel formulation			
	A	B	C	D
GG (% wt/vol)	0.5	0.75	1	1.25
GGDVS (% wt/vol)	0.25	0.375	0.5	0.625
GG/GGDVS (% wt/vol)	0.75	1.125	1.5	1.875

calculate the compressive modulus. Each value was performed in triplicate and the results were reported as the mean  $\pm$  SD.

## 2.5 | Solute diffusion testing

Gellan gum-based hydrogels prepared through casting (500  $\mu$ l, 10 mm diameter, 5 mm height) were incubated at 37°C in HG-DMEM for 24 h prior testing. Then, each hydrogel was incubated in one of the two different HG-DMEM solutions containing different-sized fluorescein isothiocyanate (FITC) conjugated dextran (Sigma-Aldrich), respectively 20-kDa dextran-FITC (1 mg/100  $\mu$ l) and 70-kDa dextran-FITC (1 mg/100  $\mu$ l). The photo-intensity of each sample was observed under a time-lapse fluorescent microscope (Axio Observer, Zeiss) for 23 h. Samples were fixed with small pins to avoid any movement during microscopic observation. Images sequences were taken at RT using a 5x objective lens. Fluorescence images were taken every 20 min over a period of 1400 min to yield a total set of 70 images.

### 2.5.1 | Image processing

All images were analyzed by MATLAB 2013. Each image was cropped to eliminate any unwanted pixel around the enclosing boundary to get equal sizes. Then, images were converted into greyscale mode. Finally, the software removed any noises in order to calculate the photo-intensity accordingly. All output data including photo-intensity, time and displacement were used to calculate the velocity of the solute through the hydrogels according to the following equation:

$$v = \frac{dx}{dt}$$

$v$  is the average velocity of molecule within the hydrogel;  $\Delta x$  is the displacement in mm;  $\Delta t$  is the change of time.

## 2.6 | Rheology testing

Inks were placed between a bottom plate and an upper probe of desired geometry (plate, conical) that exerts a rotational shear stress on the material. The rheological properties of inks were assessed with the Kinexus Pro + Rheometer (Malvern Instruments Limited, Malvern, United Kingdom). Briefly, inks were loaded on the bottom plate of the rheometer, the conical probe (4°, 40 mm) was lowered to 0.1–0.5 mm to fill the gap between the bottom plate and the probe. The thermal covers and a wet environment were set up to prevent drying. Before each measurement, inks mechanics were standardized by a 5 min initial shearing at 100  $s^{-1}$  followed by 10 min of resting. Shear thinning measurements were performed with shear rate sweep of 0.01–1000  $s^{-1}$ , at 37 °C. Yield stress measurements were performed with shear stress sweep of 0.1–1000 Pa. Thixotropic measurements were

performed by resting the sample for 60 s, shearing the sample at 100  $s^{-1}$  for 60 s, followed by resting for 60 s.

## 2.7 | 3D culture of murine myoblasts

Murine myoblasts (C2C12, Sigma, USA) were encapsulated into the pre-hydrogel solutions at a concentration of 1, 5, and 20  $\times 10^6$  cells/ml. For the initial studies, 80  $\mu$ l of the pre-hydrogel solution were casted into 48 treated well-plates. For bioprinting, 2 ml of the pre-hydrogel solution (ink or bioink) was loaded into a 2.5 ml syringe (Becton-Dickinson & CO, USA) and extruded using the parameters described in 3.7. The gellan gum-based hydrogels were formed after crosslinking by temperature decrease and addition of HG-DMEM cell culture medium. The obtained cell-laden hydrogels were cultured in vitro for up to 14 days in HG-DMEM supplemented with 10% heat-inactivated fetal bovine serum, and incubated in 5% CO<sub>2</sub> humid atmosphere at 37°C. The cell culture medium was refreshed every 2–3 days.

## 2.8 | Printing

The BioX printer (CELLINK, Sweden) was used to extrude each ink/bioink in order to print aligned filaments (10 x 10 x 0.4 mm) infilled at 18% rate. The needle size, speed, extrusion rate, and temperature used were 27G, 8 mm/s, 4  $\mu$ m/s, and 37°C, respectively. Each printed structure was built in a separate well in a 12-well plate ( $n = 6$ ). The structures were crosslinked by ionic crosslinking upon addition of the HG-DMEM cell culture medium.

## 2.9 | Cell viability analysis

A live/dead assay was utilized to assess cell viability. At each time-point, cell-laden hydrogels were incubated with a solution containing calcein AM (Ca-AM, 1 mg/ml, Invitrogen, USA), propidium iodide (PI, 1 mg/ml, Invitrogen, USA) and Hoechst (20 mM, Alfacene, USA) for an hour in a humidified atmosphere incubator with 5% CO<sub>2</sub> at 37°C. The fluorescent images of stained cells were obtained using a fluorescent microscope (Zeiss, Germany). ImageJ was used to assess viability percentage.

## 2.10 | Cytoskeletal analysis

Cell cytoskeleton was stained to assess cell morphology. At each time-point, cell-laden hydrogels were washed with phosphate buffered saline (PBS), fixated overnight with formalin 10% (Enzifarma, Italy) at 4°C, and then incubated with Phalloidin (50  $\mu$ g/mL, Sigma, USA) and 4',6-diamidino-2-phenylindole (DAPI, 1 mg/ml, Sigma, USA) for 1 h at RT. The images of cells were obtained using a confocal laser scanning microscope (Leica, Germany) equipped with axio Mrc5 cam and ZEN software and fluorescent microscope (Zeiss, Germany).

Obtained images were analyzed with ImageJ to quantify the cellular circularity.

### 2.11 | Statistical analysis

GraphPad software was used to perform statistical analysis. Data were analyzed by the Shapiro–Wilk normality test; data with a normal distribution were analyzed using one-way analysis of variance, whereas data that did not follow a normal distribution were analyzed by the Kruskal–Wallis test. Results are reported as mean  $\pm$  standard deviation  $M \pm SD$ . Significance level between groups was set for  $*p < .05$ ,  $**p < .01$ , and  $***p < .001$ ,  $****p < .0001$ .  $p$ -Values were considered significant when below .05.

## 3 | RESULTS

### 3.1 | Gellan gum-based hydrogel preparation

Twelve hydrogel formulations were developed by varying the polymer content and the tethered peptide. The polymer content was varied from 0.75% to 1.875% to develop hydrogels with different mechanical properties whereas different laminin-derived peptides (Q, V and T) were used to obtain different peptide-cell receptor affinities. The functionalization of GGDVS with Q, V and T peptides resulted in  $27.8\% \pm 6$ ,  $62.14\% \pm 3.9$ ,  $31.9\% \pm 12.9$  of efficiency, respectively, as determined by micro-BCA.

### 3.2 | Gellan gum-based hydrogel stiffness

The mechanical properties of the different hydrogel formulations were tested to conclude about the effect of stiffness over cell behavior. As shown in Figure 2, the compressive modulus of Q-based hydrogels was proportional to the polymer concentration. Accordingly, the Q-based hydrogels with the highest polymer concentration (1.875%) presented the highest compressive modulus value, which was almost four times the compressive modulus of the lowest polymer concentration (0.75% wt/vol;  $****p < .0001$ ). In fact, the increase of polymer content led to a significant increase of compressive modulus among almost all formulations, ranging from  $4.7 \pm 0.4$  kPa (0.75%) to  $20.9 \pm 3.6$  kPa (1.875%). Furthermore, both V and T-based hydrogels featured the same trend as compared to Q-based hydrogel, ranging from  $2.8 \pm 0.8$  kPa to  $21.8 \pm 5.6$  kPa ( $***p < .001$ ) and from  $4.2 \pm 2.0$  kPa to  $19.7 \pm 2.4$  kPa ( $**p < .01$ ), respectively.

### 3.3 | Molecules diffusion within gellan gum-based hydrogels

The molecular diffusion of dextran-fluorescein isothiocyanate (FITC) within the hydrogels was analyzed in order to understand the ability of encapsulated cells to receive different components of the medium within a defined time frame. In accordance, the diffusion rate of two different anionic molecular probes (20 and 70 KDa) within the hydrogels was monitored by time-lapse fluorescent microscope along 23 h of incubation (Figure 3A). Figure 3B shows the diffusion of the

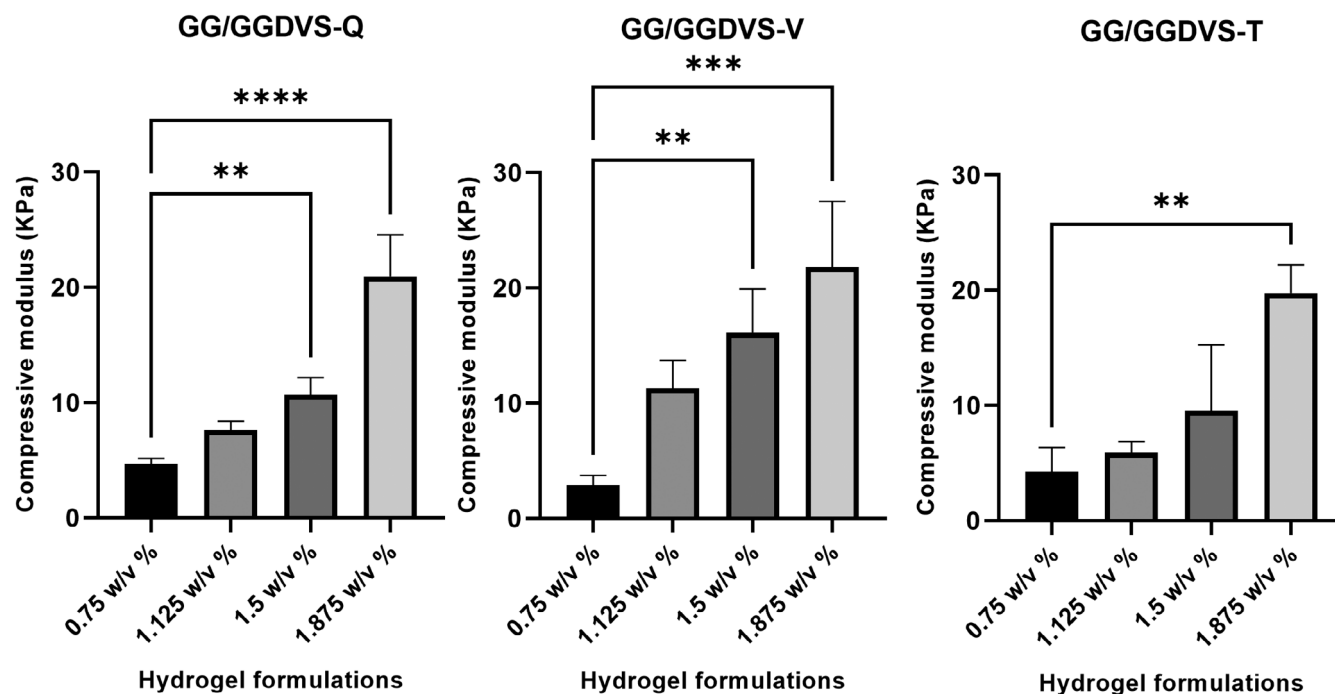


**FIGURE 2** Mechanical properties of gellan gum-based hydrogels tethered with laminin-derived peptides. Compressive modulus of gellan gum-based hydrogels after immersion in Dulbecco's Modified Eagle Medium for 48 h, at 37°C. All measurements were analyzed with Kruskal–Wallis test. Symbol (\*) indicates samples with statistically significant values ( $p < .05$ ). Data are presented by mean  $\pm$  SD.

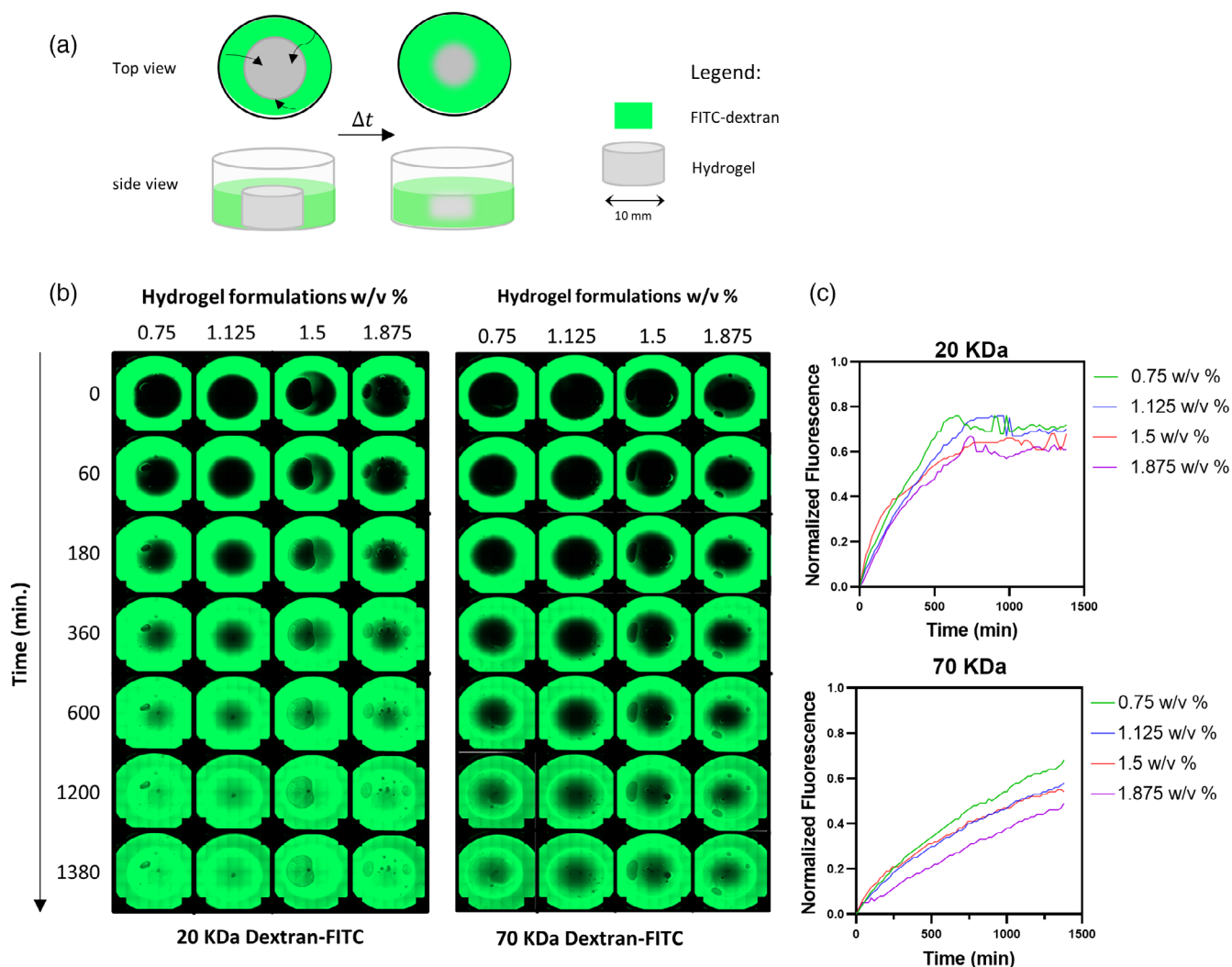


**FIGURE 3** Diffusion of fluorescein isothiocyanate (FITC)-dextran within gellan gum-based hydrogels tethered with laminin-derived peptides. (A) Schematic representation of the diffusion test. After contact with a DMEM solution containing fluorescent dextran (FITC-dextran), hydrogels uptake the FITC-dextran. (B, C) Analysis of the FITC-dextran uptake by gellan gum-based hydrogels (formulations 0.75%–1.875%) along the time (up to 1380 min), using FITC-dextran of two different molecular weights (70 and 20 KDa). (B) Representative images of the hydrogels at different time-points taken using a fluorescence inverted microscope. (C) Fluorescence intensity of each hydrogel plotted as a function of time. Spatial information was normalized from pixel to millimeter.

fluorescent dextran within each hydrogel formulation. The diffusion of the small molecular weight solute (20 KDa) within hydrogels with 0.75% of polymer increased over time along 1380 min. The solute took 360 min to cross half of the hydrogel diameter, in addition, it took roughly 50% of the whole time (680 min) till diffusing within the whole hydrogel, as depicted with a sharp turning point on the graph (Figure 3C). After reaching the center, the solute featured slightly counter diffusion out of the hydrogel, as portrayed with the graph fluctuation after reaching the turning point. Likewise, the hydrogels with 1.125% and 1.5% of polymer content featured a similar trend. However, they were slightly slower in crossing 50% of the hydrogel diameter (420 and 440 min, respectively). Thus, they reached to the center of the hydrogel after 960 and 1020 min, respectively. Hydrogels with 1.875% of polymer content featured the slowest diffusion profile as portrayed with a slower trafficking (520 min) to cross 50%

of the hydrogel, and a later turning point (1200 min) to cross almost the whole hydrogel (Figure 3C).

Apparently, 70 KDa solute trafficking was drastically slower, as no turning point was observed in none of the hydrogel formulations, indicating that the solute did not fully diffuse to the center of the hydrogel (Figure 3C). Besides, the hydrogel formulations followed a similar trend, as the solute in hydrogels with higher polymer content presented a slower diffusion to the center, as compared to the hydrogels with lower polymer content. Accordingly, hydrogels with 0.75% of polymer content took 880 min to cross to the center of the hydrogel. Meanwhile, both hydrogels with 1.125% and 1.5% took 1060 and 1080 min to cross 50% of the diameter. As anticipated, hydrogels with 1.875% had the slowest diffusion rate since the solute took the whole time (1380 min) to cross only 50% of the hydrogel diameter.

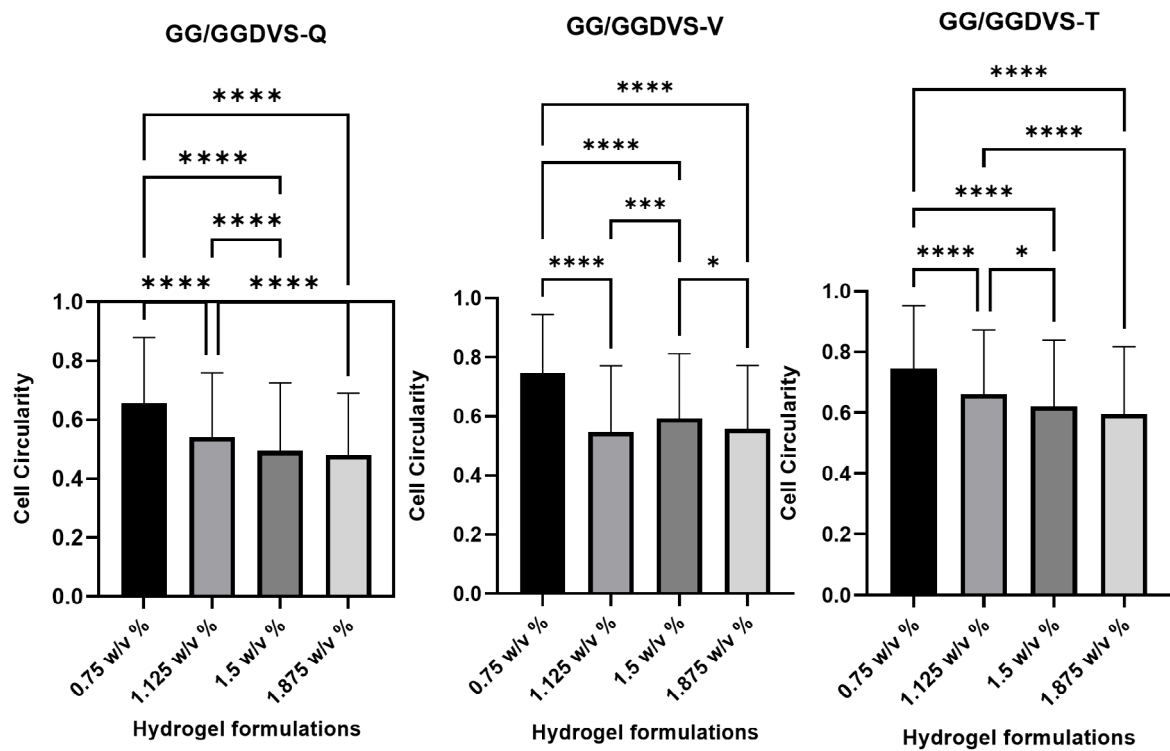
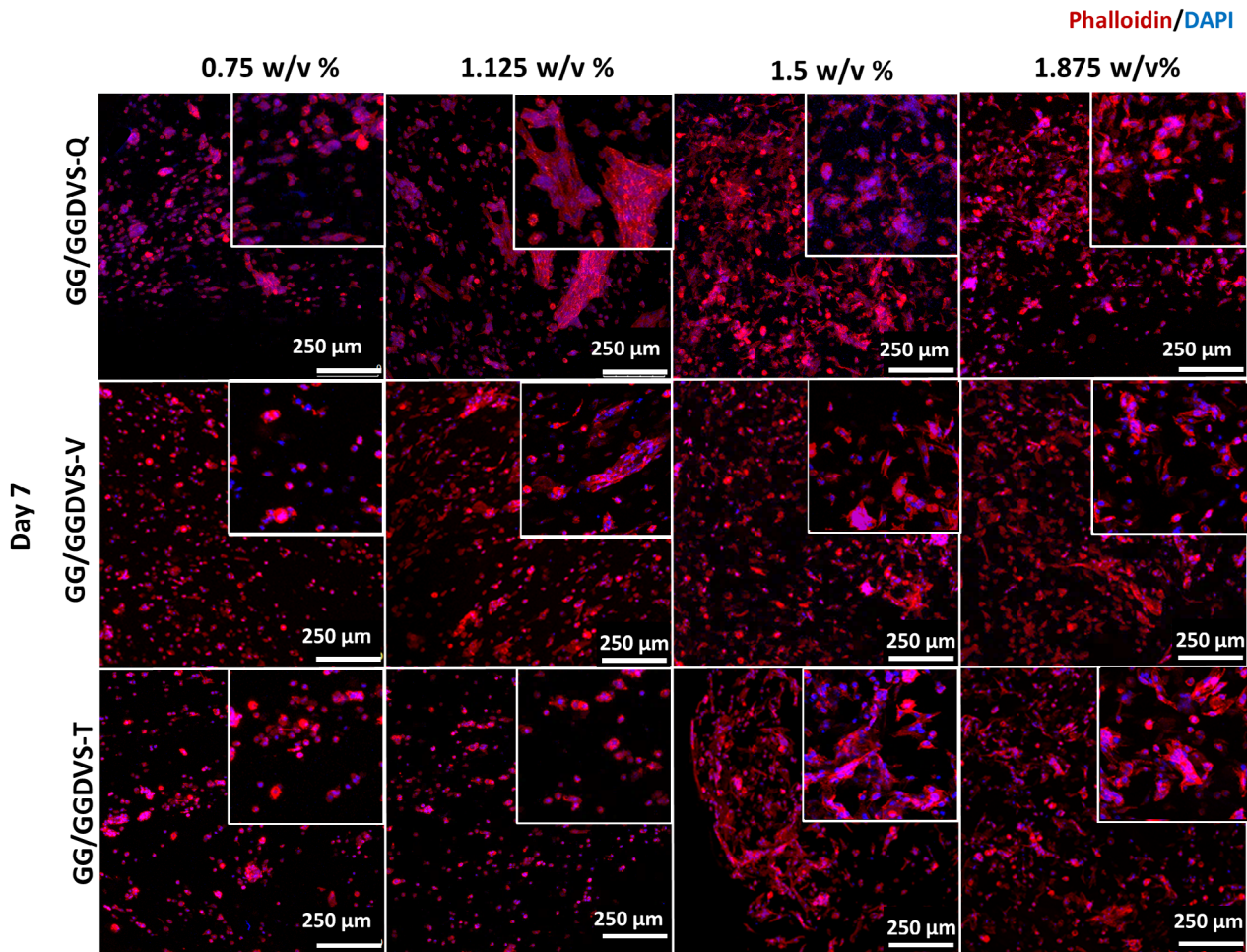


**FIGURE 4** Legend on next page.

### 3.4 | Cell adhesion within gellan gum-based hydrogels

Murine C2C12 skeletal cells were encapsulated within the different gellan gum-based hydrogels tethered with laminin-derived peptides. The cellular response was evaluated along 7 days (Figure 4). Independently of the tethered peptide, cells showed a predominant round shape in hydrogels with the lowest polymer content (0.75%), as showed by the high cell circularity (0.65–0.75). In addition, cells featured a spreading morphology in hydrogels with higher polymer content (1.125%–1.875%), showing a lower cell circularity (0.48–0.66). As an exception, cells were mostly rounded in the T-peptide tethered hydrogel (1.125%), displaying a circularity of 0.66. T-tethered hydrogels with 1.5% of polymer content featured enhanced cellular morphology (cell circularity of 0.62), as compared to the rest of formulations. In particular, in Q- and V-tethered hydrogels (1.125%), cells showed signs of cell–cell communication, as evidenced by gathered cells.

### 3.5 | Inks printability

After chemical, mechanical and biological characterization of the developed gellan gum-based hydrogels, inks with 1.125% wt/vol of polymer content were selected for printing. Initially, ink printability was assessed through oscillatory rheology analysis. Shear viscosity was recorded along a range of 0.1–1000  $s^{-1}$  of shear rate at 37°C (Figure 5A). Inks showed a non-Newtonian behavior as ink viscosity was dependent on the shear rate, as well as, a shear-thinning behavior as ink viscosity decreased with increasing shear rates. Accordingly, inks can be extruded at higher shear rates since the viscosity is lower. Independently of the peptide tethered to GG, all inks with 1.125% of polymer content showed a similar rheological behavior. Shear viscosity was also recorded along a range of 0.1–100  $s^{-1}$  of shear stress, at 37°C (Figure 5B). Shear viscosity showed values of  $10^5$  Pa s at low shear stress (1 Pa), reducing to  $10^4$  Pa s at increasing shear stress. This rheological behavior was also similar for all the ink formulations. Additionally, the thixotropic behavior of the inks was analyzed (Figure 5C). After resting for 10 min, the application of a shear rate of  $100 s^{-1}$  promoted a decrease in the shear viscosity to values of  $10^{-1}$  Pa s, indicating that inks are capable of flowing right after application of an extrusion force. Nonetheless, after application of a shearing force for 60 s, inks were not capable to recover the shear viscosity to initial values in the following 60 s, that is, presenting a shear viscosity of  $10^{-3}$  Pa s in contrast to  $10^{-6}$  Pa s, suggesting that

some shape fidelity issues may be detected. After the rheological testing, the printability was assessed using an extrusion-based printer (Figure 5D). To inspire cellular orientation, nozzle head movement was optimized to extrude in one direction (Figure 5E). Figure 5F,G shows a representative image of printed inks, right after printing (Figure 5F) and after addition of cell culture medium (Figure 5G). Three different tapered needle sizes (22, 25 and 27 g) were used to extrude the construct, showing a fiber with of  $2800 \pm 608 \mu m$ , 25 g of  $1000 \pm 126 \mu m$  and 27 g of  $787 \pm 99 \mu m$ , respectively. Moreover, constructs printed with wide sizes nozzles (22 and 25 g) featured poor geometrical retention post-printing, whereas constructs printed with 27 g presented a better shape stability and more consistency after printing (Figure 5H). No significant differences were detected on the obtained fiber using the different peptide-tethered printed inks. Nonetheless, some signs of clogging were sometimes detected during printing when using the T- and Q-peptide tethered inks. Furthermore, post-printed hydrogels showed a compressive modulus of  $1.4 \pm 0.8$  kPa.

#### 3.5.1 | Post-printing cell performance

The cell behavior within the hydrogels tethered with three different peptides Q, V and T (1.125%) was analyzed 7 days post-printing. The cell density was increased to  $5 \times 10^6$  cells/ml to improve intra cellular contact. One day after printing, cell viability ranged between 21% and 53%, specifically 21.8% in the Q-tethered hydrogel, 51.9% in the T-tethered hydrogel and 43% in the V-tethered hydrogel, (Figure 6A). After 7 days, cell viability significantly increased among most formulations, as cell showed a viability of 38%–83%, specifically 38.7% in the Q-tethered hydrogel, 63.1% in the T-tethered hydrogel and 76.4% in the V-tethered hydrogel (Figure 6A). Cell spreading was also noticed 7 days post-printing, particularly within the T- and V-tethered hydrogels (Figure 6A). Particularly, cell division was observed, since large cell clusters resultant from a single cell were detected. This was not observed in non-functionalized gellan gum-based hydrogels (Figure S1).

As an attempt to increase cell–cell communication, the cell density was increased to 20 M cells/mL of ink. For this further analysis, V-tethered hydrogels were selected since cells showed higher signs of cell viability and spreading and no clogging was detected during printing. Cell viability was not drastically altered in relation to 5 M cells/ml, showing 45.6% of viable cells at day 1 and 82.2% of viable cells at day 7 (Figure 6B). As expected, cells showed more signs of cellular elongation, polarization and cell–cell communication 7 and 14 days after

**FIGURE 4** C2c12 adhesion within gellan gum-based hydrogels tethered with laminin-derived peptides. Gellan gum was biofunctionalized with three different peptides (Q, V, T) and four different hydrogel concentrations were prepared (0.75%–1.875%). (A) Representative images of phalloidin/DAPI stained cell-laden hydrogels after 7 days of culture in DMEM and at 37°C. Phalloidin (red) and DAPI (blue) staining was used to stain the cytoskeleton and nuclei, respectively. An Olympus Fluoview FV 1000 laser confocal microscope was used to acquire the images. (B) Cell circularity quantification of each hydrogel formulation was obtained through ImageJ. A value of 1.0 indicates a perfect circle. All measurements were analyzed with ANOVA with Tukey's multiple comparisons test. DAPI, 4',6'-diamidino-2-phenylindole; DMEM, Dulbecco's Modified Eagle Medium.



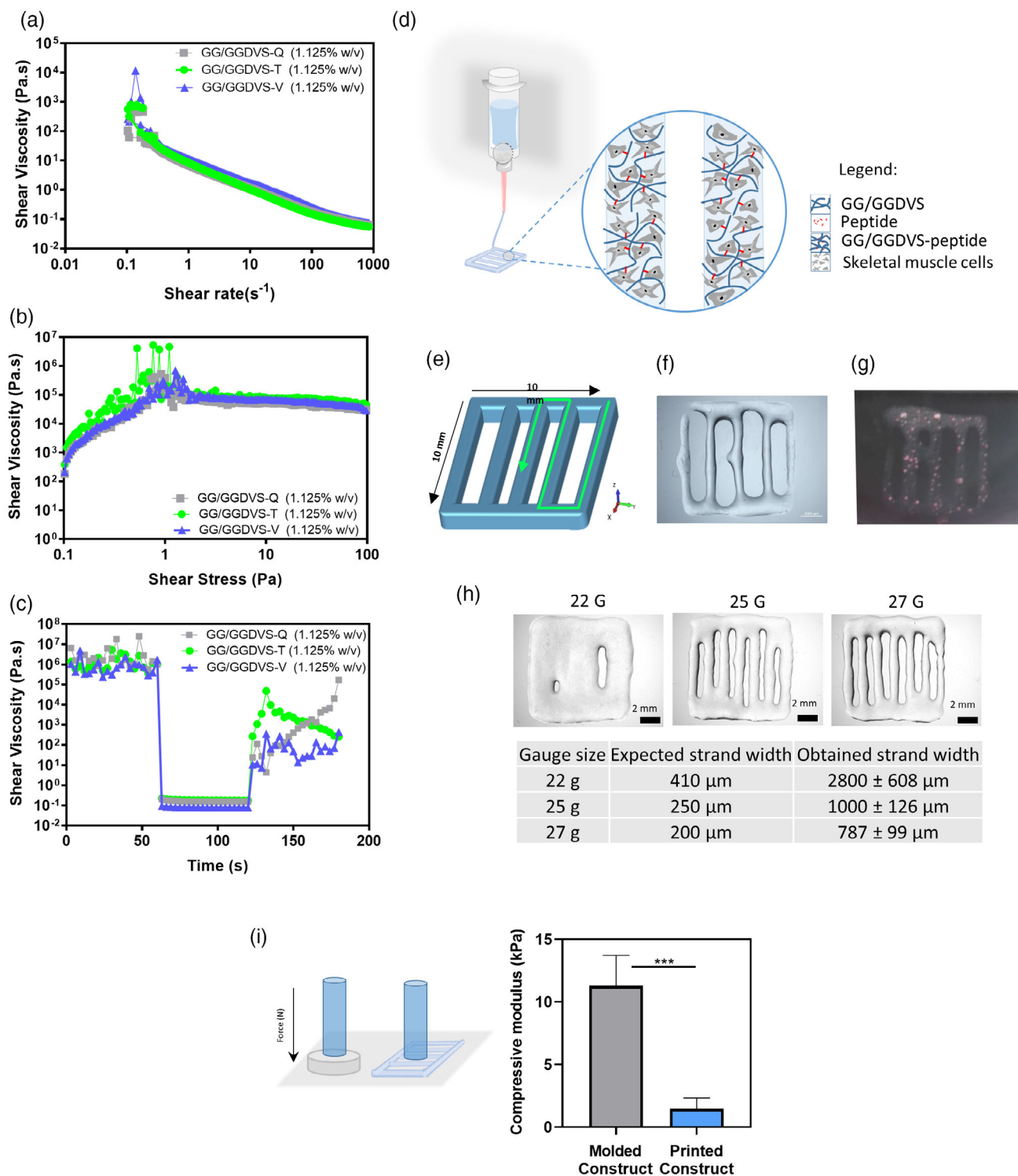


**FIGURE 5** Printability of gellan gum-based inks tethered with laminin-derived peptides using an extrusion-based printer. (A) Representative graphic of shear viscosity as function of shear rate of T, V and Q peptide tethered gellan gum-based inks (1.125%), monitored for shear rates between 0.1 and 1000  $\text{s}^{-1}$  at 37°C. (B) Representative graphic of shear viscosity as function of shear stress of T, V and Q peptide tethered gellan gum-based inks (1.125%), monitored for shear stress between 0.1 and 1000 Pa. (C) Representative graphic of shear viscosity as function of time of T, V and Q peptide tethered gellan gum-based inks (1.125%), monitored at a cycle of resting for 60 s, shearing for 60 s, and resting for 60 s. (D) Schematic representation of gellan gum-based bioinks bioprinting using a 3D extrusion-based printer. C2C12 are encapsulated within gellan gum-based inks composed of gellan gum and gellan gum biofunctionalized with a peptide. The subsequent bioink is then loaded into the extrusion-head. Parallel fibers are printed into a well-plate and left in culture for up to 14 days. (E) Illustration of the printing design used to deploy the tissue engineered construct. Macroscopic photo of the printed constructs (F) right after printing and (G) after addition of cell culture medium. (H) Strand width quantification and the corresponding printed scaffolds using nozzles of different sizes (22, 25 and 27 g). (I) Comparison of the compressive moduli between the molded and the printed construct.

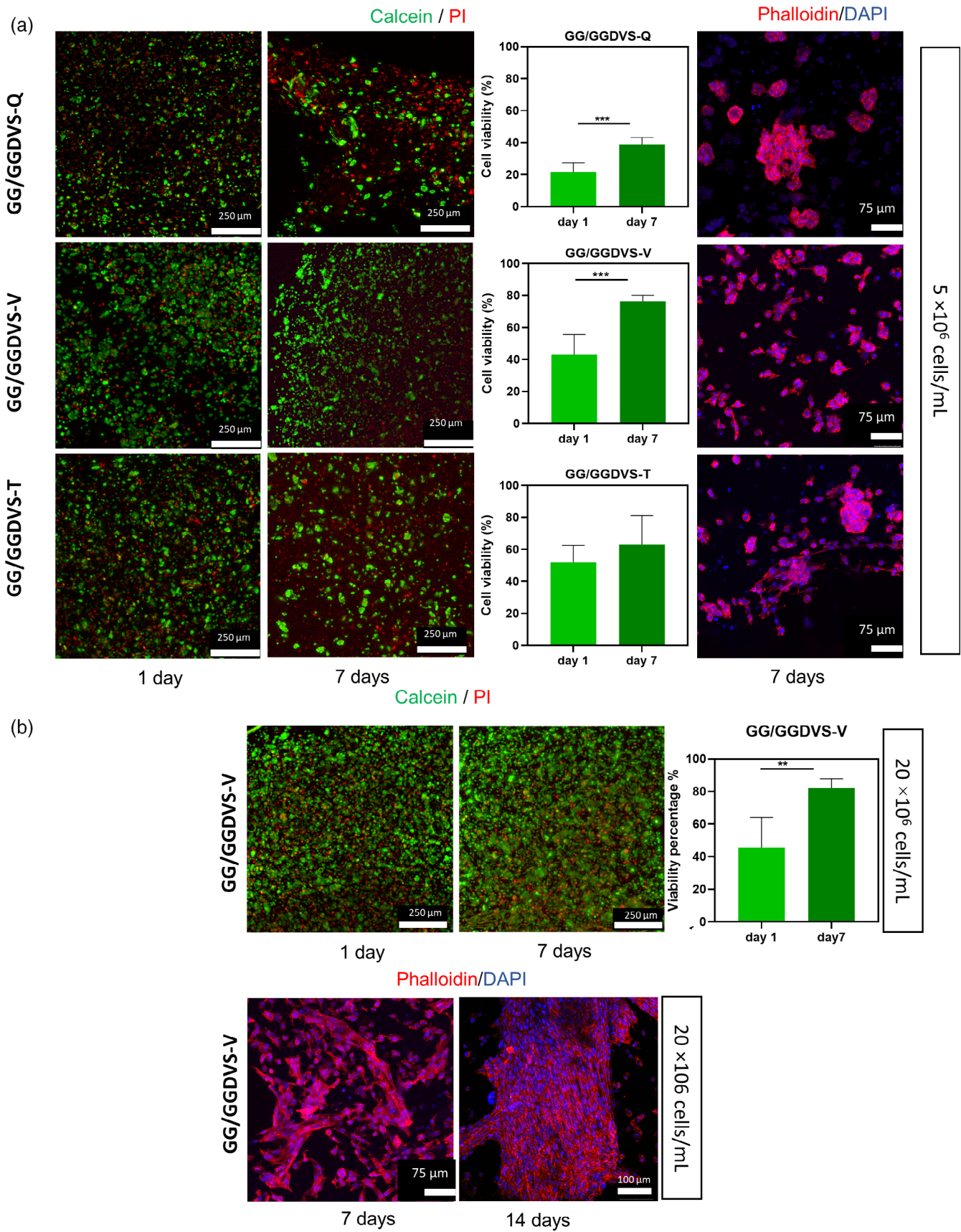


FIGURE 6 Legend on next page.

culture (Figure 6C). After the period of culture, the cell-laden hydrogels were still manageable and mechanically stable.

## 4 | DISCUSSION

Functional skeletal muscle surrogates may bring light to the treatment of skeletal muscle injuries and diseases. On one side, they can replace the damaged tissue and give biological cues for tissue regeneration. On the other side, they can work as a model for drug screening purposes. Herein, we aimed to develop a skeletal muscle surrogate by 3D culturing myoblasts in laminin-inspired biofunctionalized gellan gum-based hydrogels. First, we aimed to explore the impact of the laminin-derived peptide and polymer content (and stiffness) on the morphology of C2C12 when cultured in a 3D environment. Considering that the diffusion of molecules can be impaired in 3D environments and further influence the behavior of encapsulated cells, the diffusion of molecules was also studied for each hydrogel. Finally, the possibility of printing these tissue surrogates was assessed.

One of our goals was that gellan gum-based inks tethered with laminin-derived peptides inks would promote the adhesion of C2C12. Independently of the tethered peptide, cells featured a predominant round morphology when encapsulated in hydrogels with the lowest polymer content (0.75%) after 7 days in culture. However, cells were spreading when encapsulated in hydrogels with higher polymer content (1.125%–1.875%), and showing some signs of cell–cell communication, as evidenced in Q- and V-tethered hydrogels (1.125%). Thus, hydrogels with 1.125% seem to be favorable for cellular spreading in both Q and V peptides. Inversely, this did not apply to the T-peptide tethered gellan gum-based hydrogels where cells showed less potential for spreading and communicating. Since cells showed spreading when encapsulated in hydrogels tethered with T peptide and with higher polymer content (>1.125%), indicating that cells were capable of adhering to the T peptide, we hypothesize that the absence of cell spreading in these hydrogels is related to the stiffness of the hydrogel which, in T-tethered hydrogels, was similar to the stiffness of hydrogels with 0.75% of content.

These results were inconsistent with previous results,<sup>12</sup> where C2C12 were only spreading and differentiating on the surface of high stiff hydrogel tethered with only Q peptide. In our case, it seems that shifting from a 2D to a 3D environment influenced cellular behavior. It is recurrently reported that cells differentiate and present a more spindle-like and spreading morphology on the 2D in comparison to 3D.<sup>30–32</sup> This fact has been explained by the tighter and limited porosity found in 3D in comparison to 2D. This work corroborates these

findings as cells showed a less spreading morphology in 3D in relation to 2D. Nonetheless, cells were capable of spreading in hydrogels with different properties, not detected previously. In fact, in the 3D environment, encapsulated cells have more space to grow spatially in all dimensions and to be in contact with more hydrogel binding sites.<sup>33</sup> Therefore, it may be concluded that a rational balance between hydrogel stiffness and porosity will promote the desired cellular response,<sup>34</sup> irrespectively to the peptide type.

The stiffness of the hydrogels increased with the increase of polymer content. No significant differences were detected among the different peptide-tethered gellan gum-based hydrogels, except for the T-peptide hydrogel with 1.125% of polymer content, which showed a lower compressive modulus in relation to the Q- and T-peptide tethered gellan gum-based hydrogels. This can be explained by the difference of molecular weight and hydrophilicity among the different peptides (Table S1), which can interfere with the crosslinking of the polymer network and, consequently, with the hydrogel stiffness. The developed hydrogels presented a compressive modulus ranging between 5 and 20 kPa, a stiffness that is rather close to the range of the native skeletal muscle (8–11 kPa).<sup>34,35</sup> As expected, the mechanical properties influenced cells behavior.<sup>36,37</sup> Cell spreading was detected in most of the hydrogel formulations, except the one with lower stiffness (hydrogels with 0.75% of polymer content). Surprisingly, this result was incomparable to our previous results,<sup>12</sup> which showed enhanced cell behavior atop more stiffer hydrogel (around 30 kPa), further reinforcing the impact of encapsulation on cellular behavior.<sup>37</sup>

The ability of molecules to diffuse into the core of hydrogels is extremely important for the viability and maturation of encapsulated myoblasts. The diffusion within the hydrogel depends on multiple factors including mesh size, pore size, solute size/weight, solute-hydrogel interaction, to name a few.<sup>38</sup> To shed light on solute trafficking through the gellan gum-based hydrogels, the diffusion of FITC-dextran of different molecular sizes (20 and 70 kDa) was studied. The molecular weight of the solute is in line with the molecular weight of many growth factors and cytokines that are important for myoblast behavior. Both 20 and 70 kDa solutes were capable of diffusing within all developed hydrogels formulations, although at different diffusion rates. As anticipated, the lower molecular weighted solute was diffusing faster through the polymer mesh than higher weighted solutes. Moreover, the solutes were diffusing faster in hydrogels with lower polymer content, confirming a tighter mesh size in hydrogels with higher polymer content. Moreover, it is important to highlight that molecules in the range of 70 kDa will not be able to diffuse to the core of the hydrogels within limited period of 23 h, indicating that

**FIGURE 6** Post-printing c2c12 behavior within gellan gum-based inks tethered with laminin-derived peptides inks. (A) C2C12 ( $5 \times 10^6$  cells) were encapsulated within gellan gum-based inks (1.125%) biofunctionalized with the three different peptides (Q, V and T), printed using and extrusion-based printer and cultured up to 7 days, at standard conditions. (B) C2C12 ( $20 \times 10^6$  cells) were encapsulated within gellan gum-based inks (1.125%) biofunctionalized with T peptide, printed using and extrusion-based printer and cultured up to 14 days, at standard conditions. Cell viability and morphology were analyzed through the staining of live (calcein), dead (propidium iodide) and cytoskeleton (phalloidin). Nuclei were counter-stained with 4',6'-diamidino-2-phenylindole. Calcein/Propidium iodide images were taken using Upright Microscope with Thunder, whereas phalloidin images were taken using an Olympus Fluoview FV 1000 laser confocal microscope. Data were analyzed with T-test.

encapsulated cells in the core of the hydrogel may not have access to them in a satisfactory period time.

3D bioprinting technique was used to develop a muscle-like surrogate in order to achieve a further level of accuracy and sophistication in the engineering of skeletal muscle surrogates, as they can be constructed with further organization, complexity and automation. Rheological measurements indicated that inks were printable, since they showed a non-newtonian, shear-thinning and thixotropic behavior. This was further confirmed after testing their printability using an extrusion-based printer. Accordingly, gellan gum-based hydrogel filaments were printed in a unified direction in order to mimic the anisotropic structure of native myotubes. Among each peptide-based hydrogel, all formulations were printable under stable temperature (37°C) and extrusion rate. Nonetheless, some clogging issues were reported during printing with the Q and T-peptide tethered gellan gum-based inks. As expected from the rheological measurements, some fiber spreading was detected after fiber deposition, thus obtaining strand width higher than the expected. Thus, to obtain better printing resolution, a narrower gauge size (27 g) was selected for the further studies. The printed construct showed a lower compressive modulus in relation to the molded one, as expected, since it featured different dimensions as compared to molded construct, i.e. instead of a bulk and a compact hydrogel, the printed hydrogel comprised inner spacing between the fibers and a thinner thickness.

Taking in consideration that the use of needles with small diameter could affect cell viability, as a higher pressure is provoked in the ink to be extruded and therefore a higher shear stress is applied on the encapsulated cells, the viability of printed cells was analyzed. Cell viability was dependent on the ink, as cell viability was severely affected in Q-tethered hydrogels after printing. Since no significant differences were detected in shear viscosity among the different ink formulations, we may hypothesize that the intermittent clogging during printing might have affected cell viability. Cells in V and T-tethered gellan gum-based hydrogels showed higher viability after printing, but still presenting a moderate amount of cell death (50%–60%). This was possibly related to the shear stress applied at the nozzle tip during printing, as previously reported.<sup>40</sup> After 7 days of culture, cell viability remarkably increased, particularly in V-tethered hydrogels.

Although printed cells were viable and adherent 7 days post-printing, printed cells were not resembling the architecture of the skeletal muscle. It was hypothesized that the cell density ( $5 \times 10^6$  cells/ml) was not enough to promote cell–cell communication and promote the alignment existing the skeletal muscle, as also reported by others.<sup>41</sup> Thus, we selected V-based inks to encapsulate  $20 \times 10^6$  cell/ml and analyze cell behavior, since V-based inks showed no clogging issues and presented high cell viability and adhesion, in comparison to the other inks (gellan gum-based inks tethered with T or Q). At this cell density, cell behavior drastically changed. Cells were in contact among them and showed a spread and aligned morphology with a few hundreds of micrometers long, not previously detected using a lower cell density. This was in line with what was observed elsewhere<sup>15,42</sup> and can be explained by the enhanced cell–cell contact that promotes an enhanced inter-cellular communication, as previously reported by others.<sup>43</sup> Thus,

the potential of this construct to mature into a functional contractile muscle surrogate will be further evaluated in the future. Moreover, new printing technologies (e.g. printing using a supporting bath) will be explored to attain a higher degree of shape-fidelity, and to achieve a multilayered construct.

## 5 | CONCLUSION

The main goal of this work was to develop a hydrogel formulation that would be printable and that would promote the viability and spreading of skeletal muscle cells post-printing. Thus, different gellan gum-based hydrogels were developed by tethering different laminin-derived peptides (Q, V and T) and by varying the polymer content. The most promising hydrogel formulation was selected after analysis of cell adhesion and molecules diffusion within the different hydrogel formulations. C2C12 showed a spindle-like morphology after 7 days of encapsulation, independently of the laminin-derived peptide tethered to gellan gum, but only in hydrogels with higher polymer amount (1.125%–1.875%). Since molecules diffusion was favored in hydrogels with lower polymer content (0.75%–1.125%), hydrogels with 1.125% of polymer content were selected for printing. Gellan gum-based inks tethered with the different laminin-derived peptides (1.125%) showed a non-newtonian, shear-thinning and thixotropic behavior promising for printing, as confirmed after using an extrusion-based printer. Cells were printed at a cell density of 5 M cell/ml, remaining viable and spreading 7 days after printing, but no showing significant signs of cell–cell communications. Thus, V-tethered gellan gum-based inks were selected to encapsulate cells at a higher density (20 M cell/ml), since T- and Q-peptide tethered gellan gum-based inks experienced some signs of clogging during printing and the viability of skeletal muscle cells within Q-peptide tethered gellan gum-based inks was affected. Cells were viable and spreading 7 days post-printing and showed a higher cell–cell communication, spreading morphology and alignment when the cell density was increased to  $20 \times 10^6$  cell/ml. Taken together, myoblast laden in laminin-inspired gellan gum-based hydrogels may shed some light on the function of skeletal muscle cells within a 3D microenvironment and might serve as a skeletal muscle model for screening the cellular response *in vitro*.

## ACKNOWLEDGMENTS

Omar Alheib acknowledge the financial support from the Portuguese Foundation for Science and Technology (FCT) for the PhD grant FCT PD/BD/128090/2016 under TERM program PD/59/2013. Lucilia P. da Silva would like to acknowledge FCT—Fundação para a Ciência e a Tecnologia, I.P. and, when eligible, by COMPETE 2020 FEDER funds, under the Scientific Employment Stimulus—Individual Call (CEEC Individual)—2020.01541.CEECIND/CP1600/CT0024. Reem Sweid for analyzing images with MATLAB software and assisting with graphical results.

## DATA AVAILABILITY STATEMENT

The raw/processed data required to reproduce these findings cannot be shared at this time due to technical limitations.

## ORCID

Omar Alheib  <https://orcid.org/0000-0003-4547-9636>

Yun Hee Youn  <https://orcid.org/0000-0003-0544-3719>

## REFERENCES

- Gillies AR, Lieber RL. Structure and function of the skeletal muscle extracellular matrix. *Muscle Nerve*. 2011;44:318-331. doi:10.1002/mus.22094
- Fernandes TL, Pedrinelli A, Hernandez AJ. Muscle injury—physiopathology, diagnosis, treatment and clinical presentation. *Rev Bras Ortop*. 2011;46:247-255. doi:10.1016/s2255-4971(15)30190-7
- Dumont NA, Bentzinger CF, Sincennes MC, Rudnicki MA. Satellite cells and skeletal muscle regeneration. *Compr Physiol*. 2015;5:1027-1059. doi:10.1002/cphy.c140068
- Parker MH. The altered fate of aging satellite cells is determined by signaling and epigenetic changes. *Front Genet*. 2015;6:1-7. doi:10.3389/fgene.2015.00059
- Motohashi N, Asakura A. Muscle satellite cell heterogeneity and self-renewal. *Front Cell Dev Biol*. 2014;2:1-11. doi:10.3389/fcell.2014.00001
- Baker BA. An old problem: aging and skeletal-muscle-strain injury. *J Sport Rehabil*. 2017;26:180-188. doi:10.1123/jsr.2016-0075
- Ramos LA, de Carvalho RT, Abdalla RJ, Ingham SJMN. Surgical treatment for muscle injuries. *Curr Rev Musculoskelet Med*. 2015;8:188-192. doi:10.1007/s12178-015-9272-0
- Qazi TH, Mooney DJ, Pumberger M, Geißler S, Duda GN. Biomaterials based strategies for skeletal muscle tissue engineering: existing technologies and future trends. *Biomaterials*. 2015;53:502-521. doi:10.1016/j.biomaterials.2015.02.110
- Fischer KM, Scott TE, Browe DP, et al. Hydrogels for skeletal muscle regeneration. *Regen Eng Transl Med*. 2020;7:1-9. doi:10.1007/s40883-019-00146-x
- Scelsi A, Bochicchio B, Smith A, et al. Tuning of hydrogel stiffness using a two-component peptide system for mammalian cell culture. *J Biomed Mater Res - Part A*. 2019;107:535-544. doi:10.1002/jbm.a.36568
- Rowley JA, Mooney DJ. Alginate type and RGD density control myoblast phenotype. *J Biomed Mater Res*. 2002;60:217-223. doi:10.1002/jbm.1287
- Alheib O, da Silva LP, Caballero D, et al. Micropatterned gellan gum-based hydrogels tailored with laminin-derived peptides for skeletal muscle tissue engineering. *Biomaterials*. 2021;279:121217. doi:10.1016/j.biomaterials.2021.121217
- Khetan S, Burdick JA. Patterning network structure to spatially control cellular remodeling and stem cell fate within 3-dimensional hydrogels. *Biomaterials*. 2010;31:8228-8234. doi:10.1016/j.biomaterials.2010.07.035
- Kang HW, Lee SJ, Ko IK, Kengla C, Yoo JJ, Atala A. A 3D bioprinting system to produce human-scale tissue constructs with structural integrity. *Nat Biotechnol*. 2016;34:312-319. doi:10.1038/nbt.3413
- Distler T, Solisito AA, Schneidereit D, Friedrich O, Detsch R, Boccaccini AR. 3D printed oxidized alginate-gelatin bioink provides guidance for C2C12 muscle precursor cell orientation and differentiation via shear stress during bioprinting. *Biofabrication*. 2020;12:045005. doi:10.1088/1758-5090/ab98e4
- Bandyopadhyay A, Dewangan VK, Vajanthri KY, Poddar S, Mahto SK. Easy and affordable method for rapid prototyping of tissue models in vitro using three-dimensional bioprinting, Biocybern. *Biomed Eng*. 2018;38:158-169. doi:10.1016/j.bbe.2017.12.001
- da Silva LP, Santos TC, Rodrigues DB, et al. Stem cell-containing hyaluronic acid-based spongy hydrogels for integrated diabetic wound healing. *J Invest Dermatol*. 2017;137:1541-1551. doi:10.1016/j.jid.2017.02.976.
- Silva LPD, Pirraco RP, Santos TC, et al. Neovascularization induced by the hyaluronic acid-based spongy-like hydrogels degradation products. *ACS Appl Mater Interfaces*. 2016;8:33464-33474. doi:10.1021/acsami.6b11684
- M. T. Cerqueira, L. Pereira Da Silva, T. C. Santos, R. P. Pirraco, V. M. Correlo, R. L. Reis, A. P. Marques. Gellan gum-hyaluronic acid spongy-like hydrogels and cells from adipose tissue synergize promoting neovascularization. *ACS Appl Mater Interfaces*. 2014:19668-79. doi:10.1021/am504520j
- Cerqueira MT, Da Silva LP, Santos TC, et al. Human skin cell fractions fail to self-organize within a gellan gum/hyaluronic acid matrix but positively influence early wound healing. *Tissue Eng - Part A*. 2014;20:1369-1378. doi:10.1089/ten.tea.2013.0460
- Vieira S, Morais AS, Garet E, et al. Self-mineralizing calcium-enriched methacrylated gellan gum beads for bone tissue engineering. *Acta Biomater*. 2019;93:74-85. doi:10.1016/j.actbio.2019.01.053
- Srisuk P, Berti FV, Da Silva LP, Marques AP, Reis RL, Correlo VM. Electroactive Gellan gum/polyaniline spongy-like hydrogels. *ACS Biomater Sci Eng*. 2018;4:1779-1787. doi:10.1021/acsbomaterials.7b00917
- Berti FV, Srisuk P, Da Silva LP, Marques AP, Reis RL, Correlo VM. Synthesis and characterization of electroactive Gellan gum spongy-like hydrogels for skeletal muscle tissue engineering applications. *Tissue Eng - Part A*. 2017;23:1-12. doi:10.1089/ten.tea.2016.0430
- da Silva LP, Jha AK, Correlo VM, Marques AP, Reis RL, Healy KE. Gellan gum hydrogels with enzyme-sensitive biodegradation and endothelial cell biorecognition sites. *Adv Healthc Mater*. 2018;7:1700686. doi:10.1002/adhm.201700686
- M. P. Hoffman, M. Nomizu, E. Roque, S. Lee, D. W. Jung, Y. Yamada, H. K. Kleinman, Laminin-1 and Laminin-2 G-domain synthetic peptides bind syndecan-1 and are involved in acinar formation of a human submandibular gland cell line, *J Biol Chem*. 1998;273:28633-41. doi:10.1074/jbc.273.44.28633
- Larraín J, Cizmeci-Smith G, Troncoso V, Stahl RC, Carey DJ, Brandan E. Syndecan-1 expression is down-regulated during myoblast terminal differentiation: modulation by growth factors and retinoic acid. *J Biol Chem*. 1997;272:18418-18424. doi:10.1074/jbc.272.29.18418
- Stevenson M, Hale ABH, Hale SJ, et al. Incorporation of a laminin-derived peptide (SIKVAV) on polymer-modified adenovirus permits tumor-specific targeting via  $\alpha 6$ -integrins. *Cancer Gene Ther*. 2007;14:335-345. doi:10.1038/sj.cgt.7701022
- Freitas VM, Vilas-Boas VF, Pimenta DC, et al. SIKVAV, a laminin  $\alpha 1$ -derived peptide, interacts with integrins and increases protease activity of a human salivary gland adenoid cystic carcinoma cell line through the ERK 1/2 signaling pathway. *Am J Pathol*. 2007;171:124-138. doi:10.2353/ajpath.2007.051264
- Farrukh A, Ortega F, Fan W, et al. Bifunctional hydrogels containing the laminin motif IKVAV promote neurogenesis. *Stem Cell Rep*. 2017;9:1432-1440. doi:10.1016/j.stemcr.2017.09.002
- Mabry KM, Payne SZ, Anseth KS. Microarray analyses to quantify advantages of 2D and 3D hydrogel culture systems in maintaining the native valvular interstitial cell phenotype. *Biomaterials*. 2016;74:31-41. doi:10.1016/j.biomaterials.2015.09.035
- Chitcholtan K, Asselin E, Parent S, Sykes PH, Evans JJ. Differences in growth properties of endometrial cancer in three dimensional (3D) culture and 2D cell monolayer. *Exp Cell Res*. 2013;319:75-87. doi:10.1016/j.yexcr.2012.09.012
- Pineda ET, Nerem RM, Ahsan T. Differentiation patterns of embryonic stem cells in two versus three dimensional culture. *Cells Tissues Organs*. 2013;197:399-410. doi:10.1159/000346166
- Baker BM, Chen CS. Deconstructing the third dimension-how 3D culture microenvironments alter cellular cues. *J Cell Sci*. 2012;125:3015-3024. doi:10.1242/jcs.079509

34. O'Brien FJ. Biomaterials & scaffolds for tissue engineering. *Mater Today*. 2011;14:88-95. doi:[10.1016/S1369-7021\(11\)70058-X](https://doi.org/10.1016/S1369-7021(11)70058-X)
35. Y. Yoshikawa, T. Yasuike, A. Yagi, T. Yamada, Transverse elasticity of myofibrils of rabbit skeletal muscle studied by atomic force microscopy. 1999. <http://www.ideallibrary.com>
36. Engler AJ, Griffin MA, Sen S, Bönnemann CG, Sweeney HL, Discher DE. Myotubes differentiate optimally on substrates with tissue-like stiffness: pathological implications for soft or stiff microenvironments. *J Cell Biol*. 2004;166:877-887. doi:[10.1083/jcb.200405004](https://doi.org/10.1083/jcb.200405004)
37. Engler AJ, Sen S, Sweeney HL, Discher DE. Matrix elasticity directs stem cell lineage specification. *Cell*. 2006;126:677-689. doi:[10.1016/j.cell.2006.06.044](https://doi.org/10.1016/j.cell.2006.06.044)
38. Ahearne M. Introduction to cell-hydrogel mechanosensing. *Interface Focus*. 2014;4:20130038. doi:[10.1098/rsfs.2013.0038](https://doi.org/10.1098/rsfs.2013.0038)
39. Zustiak SP, Boukari H, Leach JB. Solute diffusion and interactions in cross-linked poly(ethylene glycol) hydrogels studied by fluorescence correlation spectroscopy. *Soft Matter*. 2010;6:3609-3618. doi:[10.1039/c0sm00111b](https://doi.org/10.1039/c0sm00111b)
40. Emmermacher J, Spura D, Cziommer J, et al. Engineering considerations on extrusion-based bioprinting: interactions of material behavior, mechanical forces and cells in the printing needle. *Biofabrication*. 2020;12:025022. doi:[10.1088/1758-5090/AB7553](https://doi.org/10.1088/1758-5090/AB7553)
41. Kim JH, Seol YJ, Ko IK, et al. 3D bioprinted human skeletal muscle constructs for muscle function restoration. *Sci Rep*. 2018;8:12307. doi:[10.1038/s41598-018-29968-5](https://doi.org/10.1038/s41598-018-29968-5)
42. Kang MS, Il Kang J, Le Thi P, et al. Three-dimensional printable gelatin hydrogels incorporating graphene oxide to enable spontaneous myogenic differentiation. *ACS Macro Lett*. 2021;10:426-432. doi:[10.1021/ACSMACROLETT.OC00845](https://doi.org/10.1021/ACSMACROLETT.OC00845)
43. Tanaka K, Sato K, Yoshida T, et al. Evidence for cell density affecting C2C12 myogenesis: possible regulation of myogenesis by cell-cell communication. *Muscle Nerve*. 2011;44:968-977. doi:[10.1002/mus.22224](https://doi.org/10.1002/mus.22224)

#### SUPPORTING INFORMATION

Additional supporting information may be found in the online version of the article at the publisher's website.

**How to cite this article:** Alheib O, da Silva LP, Youn YH, Kwon IK, Reis RL, Correlo VM. 3D bioprinting of gellan gum-based hydrogels tethered with laminin-derived peptides for improved cellular behavior. *J Biomed Mater Res*. 2022;1-14. doi:[10.1002/jbm.a.37415](https://doi.org/10.1002/jbm.a.37415)